

CHAPTER 3 DEVELOPMENT OF KBMF-PR ANALYTICAL MODEL

3.1 Introduction

In modeling KBMF with PR connections, the nonlinear behavior of PR connections and knee braces elements are essential. PR connections are more flexible than fixed-end connections. They will decrease the stiffness of the frame. On the other hand, knee braces can help the frame in resisting the lateral deformation. The model must be able to accurately predict the nonlinear behavior of the connection and buckling/yielding of the knee braces. The model of the PR connections and the knee braces are explained in the following sections. All of the models described herein were implemented in a computer program PERFORM-3D [17].

A mechanical model of PR connections was proposed. This model uses a component-based method that is practical for modeling the complex behavior of many components in the connection. The nonlinear behavior of each component in the connection is considered. Afterward, an appropriate analytical model was developed; it was then used to determine the response of a KBMF with PR connections. Two different types of knee braces were considered in this study: regular buckling braces and buckling-restrained braces (BRBs). This type of structural system has not been conceived or used before. Thus, to verify the behavior of this system, the analytical results from the model were compared with experimental results of a prototype test specimen under cyclic loading. Finally, the hysteretic behavior of the frame using two different types of braces, as mentioned earlier, were studied, compared, and discussed.

3.2 Modeling components of KBMF with PR connections

In this study, a mechanical model was employed to simulate the beam-to-column connection. A cyclic behavior of a PR connection can be predicted by using a component-based method. The main concept of this method is to combine many deformable components to represent a single structural entity. The model has the capability to simulate beam-to-column joint elements under cyclic loading. In this study, a bolted top and seat angle connection with double web angles was chosen to be used as beam-to-column joints in KBMF. Properly detailed, these connections exhibit large ductility and energy dissipation capacity. The nonlinear behaviors of the deformable components such as angles and bolts were considered. All components of this connection can be modeled by using one-dimension inelastic springs and are formulated in the force-displacement relationship.

The component-based mechanical model for a top and seat bolted angle connection with double web angles as proposed by Kim et al.[14] was used. The model considers key deformation components including the nonlinear behavior of the angles, the contact and detachment between the face of the column flange and connecting angles, and the column panel zone. The schematic of a bolted top and seat angle connection with double web angles and the analytical model is shown in Figure 3.1.

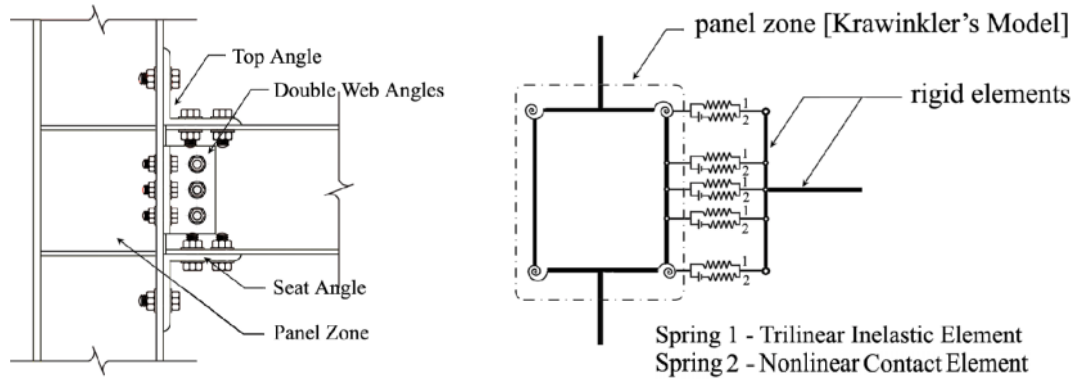


Figure 3.1 Top and Seat Bolted Angle Connections with Double Web Angles and Mechanical Model as used by Kim et al. [14].

3.2.1 Top, Bottom and Web Angles

Top-and-bottom angle connections under moment can be simplified to bolted-angles under tension and compression loading. A behavioral hysteresis model of bolted-angles based on Kim et al. [14] is discussed in this section. A trilinear inelastic element in the model (Spring 1 in Figure 3.1) represents bolts and angles combined in a single element. The force–displacement relationship of the spring can be found by considering a model shown in Figure 3.2. As can be seen, the L-shape model represents one half of the double connection. The behavior of the angles is considered when push-pull load is assigned. The thickness of the angle is the key in defining the stiffness and the strength of the element. The assumptions of the model parameters are directly derived from the experimental results. Some higher order effects are ignored. The interaction between the bolts and angles is considered and the prying action is included in the large-displacement analyses.

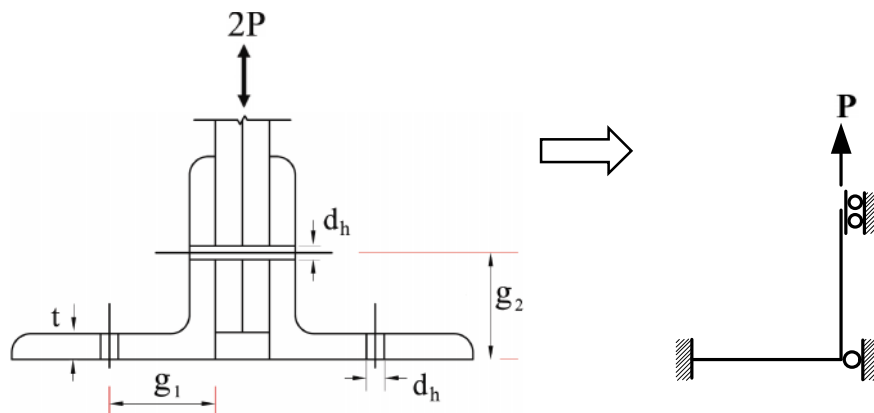


Figure 3.2 Idealized Model of Angle by Kim et al [14].

A tri-linear load-deformation relationship as shown in Figure 3.4 is employed for this element. The stiffness and the strength of this element depend on the geometry and material properties of each angle and bolt. The process of deformation is simplified into four stages including an elastic stage, a transition stage, a mechanism stage and a post-yielding stage. The tri-linear curve starts in the elastic stage assuming that the column bolt center line of the outstanding angle leg is fixed. A simple structural analysis could be used to derive the stiffness. The deformation behavior in this stage is controlled by the initial stiffness (K_o) up to the first yield displacement Δ_y , when the first plastic hinge forms at the column bolt center line of the outstanding leg of the angle which the force reaches the first yielding load (P_y). After the load reaches the first yielding value, the transition stage begins.

The transition stiffness (K_t) for this deformation stage can be calculated by the elastic analysis under the assumption that the plastic hinge has formed. The second yielding load (P_s) occurs when a mechanism forms and can be computed by the plastic mechanism analysis. Beyond this point, the load increases due to strain hardening only with the post-yielding stiffness (K_u).

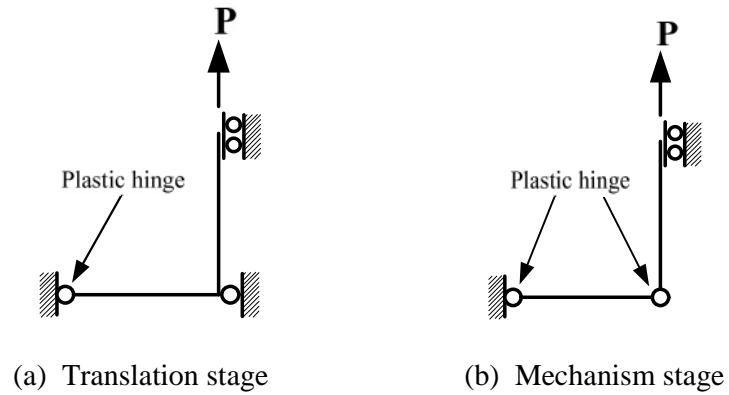


Figure 3.3 Deformation Process as presented by Kim et al [14].

Based on Kim et al. [14], the key parameters including the initial stiffness (K_o), the first yielding load (P_y), the transition stiffness (K_t), and the second yielding load (P_s) can be computed using:

$$K_o = \frac{12EI}{g_1^3} \left[1 - \frac{3g_1}{4(g_1 + g_2)} \right] \quad (3.1)$$

$$P_y = \frac{4g_1 + g_2}{g_1(2g_1 + g_2)} M_y \quad (3.2)$$

$$K_t = \frac{12EI}{(g_1 - t)^2} \left[\frac{1}{4(g_t - t) + 3g_2} \right] \quad (3.3)$$

and

$$P_s = \frac{2M_p}{g_1 - t - \frac{d_h}{2}} \quad (3.4)$$

where, g_1 and g_2 are the distances from the back of the angle to the center line of the bolts on the column and on the beam, respectively, t is the thickness of the angle, M_y is the yield moment capacity of the angle section, M_p is the plastic moment capacity of the angle section, d_h is the diameter of the bolt hole, w is the angle width per bolt, EI is bending rigidity of the angle. The post-yielding stiffness (K_u) is assumed to be 3% of the initial stiffness as proposed by Kim et al. [14], that is:

$$K_u = 0.03 \times K_0 \quad (3.5)$$

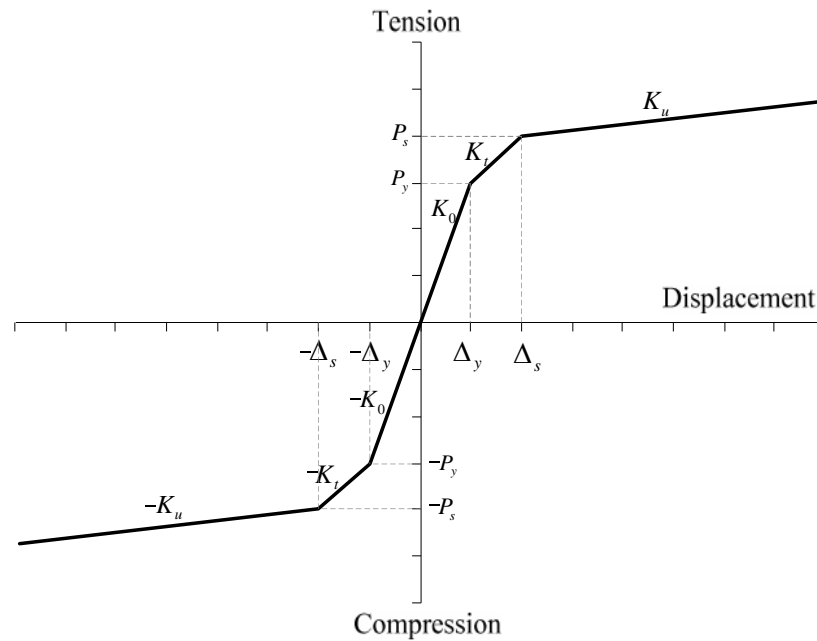


Figure 3.4 Force-Displacement Relationship of Trilinear Inelastic Element.

3.2.2 Contact and detachment of Angle with Column Flange

The contact and detachment between angles and the column flange can be represented by a Gap element (spring 2 in Figure 3.1). This element carries a compression load only, and has zero stiffness when subjected to a tension force as shown in Figure 3.5. This element introduces pinching behavior in the hysteretic response. The pinching occurs due to the change in the stiffness when contact and detachment occur. The stiffness of compression during the contact is based on the stiffness of the column web in compression. The stiffness of the column web in compression used in this study was based on the equation proposed by Faella et al. [15]:

$$K_{cwc} = E \frac{[2t + 0.6r_a + 2(t_{cf} + s)]t_{cw}}{d_c} \quad (3.6)$$

In the above formula, the value of s is equal to r_c for a rolled section or $2a_c$ for a built-up section where r_c and a_c are the web-to-flange radius of the column and the throat thickness of the welds, respectively.

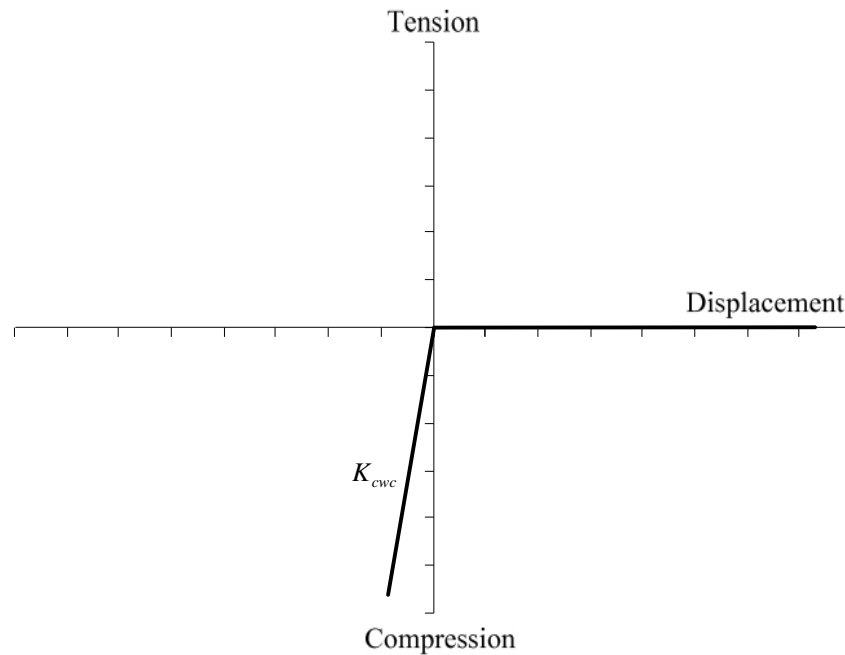


Figure 3.5 Force-Displacement Relationship of Nonlinear Contact Element.

Figure 3.6 shows the process of contact and detachment of the angle. Rigid solid lines and rigid dotted lines represent the column flange face and the beam end, respectively. In steps 1, 4, 5 and 8 the stiffness is increased when the angles contacted the column face which resists by the column web. On the other hand, the column web is relaxed in steps 2 to 3 and 6 to 7 causing the stiffness to decrease.

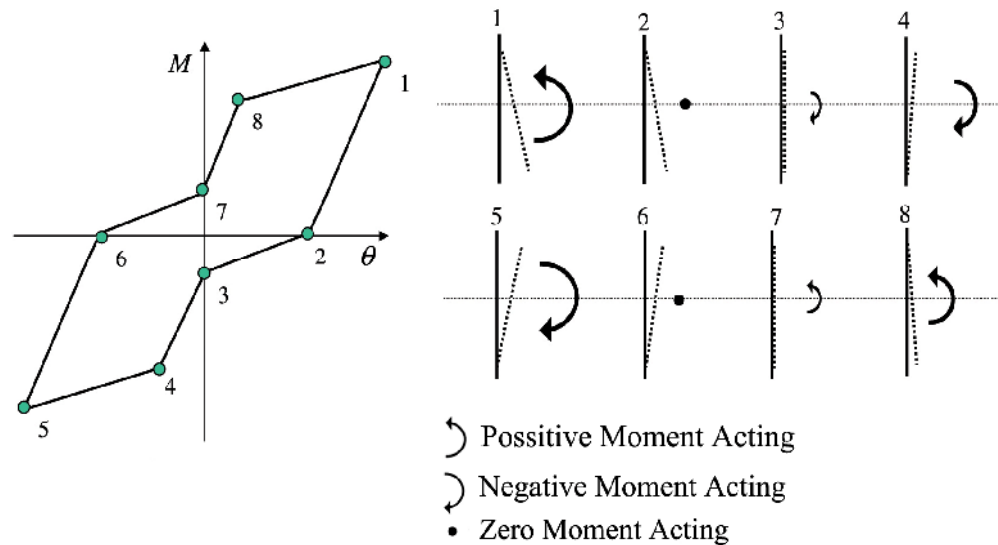


Figure 3.6 Diagram of Contact and Detachment [14].

3.2.3 Column Panel zones

The panel zones could be modeled by using the connection panel zone components from the component library of PERFORM-3D. This component utilizes the strength and stiffness model following Krawinkler et al.[16]. The model consists of an elastic-perfectly plastic shear panel connected by rigid bars and linked with rotational springs at the four corners (shown in Figure 3.1). Altogether, these springs provide a bi-linear force-deformation relationship with strain hardening.

3.2.4 Beams and Columns

The beams and columns in the frame were modeled by using the inelastic beam and column elements. These elements use lumped plasticity concept that simulates the plastic hinges with a bi-linear force deformation relationship. The plastic moment hinge model was used in the beam component, and the P-M rotation hinge was used in the column components. Elastic-plastic hysteretic behavior with strain hardening was used to represent the inelastic response of the beam-column hinge. For KBMF system, Sechai [21] recommends that the appropriate value of steel-hardening for analysis be in the order of 8% of the initial stiffness. This large strain hardening value is due to the fact that the beam segments between the knee braces are relatively short.

3.2.5 Regular Buckling Braces

Knee-braces are important elements that affect the global strength and stiffness of the frame system. The elements exhibit a complex post-buckling strength degradation pattern which affects the overall hysteretic response of the structure. Pinching observed in the hysteretic loops of the test specimens is due primarily to the strength degradation after buckling and the increase in the member length after the element yielding [21].

In this study, inelastic bar elements with buckling material in PERFORM-3D material library were used in modeling regular buckling braces. The post-buckling strength, reloading path after buckling and the strength degradation after buckling are considered under the buckling material. In tension, the element yields at the yield strength of the element without strain hardening. In compression, the compressive strength equals the buckling strength in the first cycle. After first buckling, the compressive strength is gradually reduced in subsequent cycles to the post-buckling strength which is specified by a strength reduction factor. The strength reduction factor for a stocky compression member (kL/r less than 30) was found from experiments [22] to be approximately 80% of the initial buckling strength. The backbone curve used in the modeling of buckling braces is shown in Figure 3.7. Experimental results [22] show that the first fracture occurred in knee braces approximately at the ductility of 4.

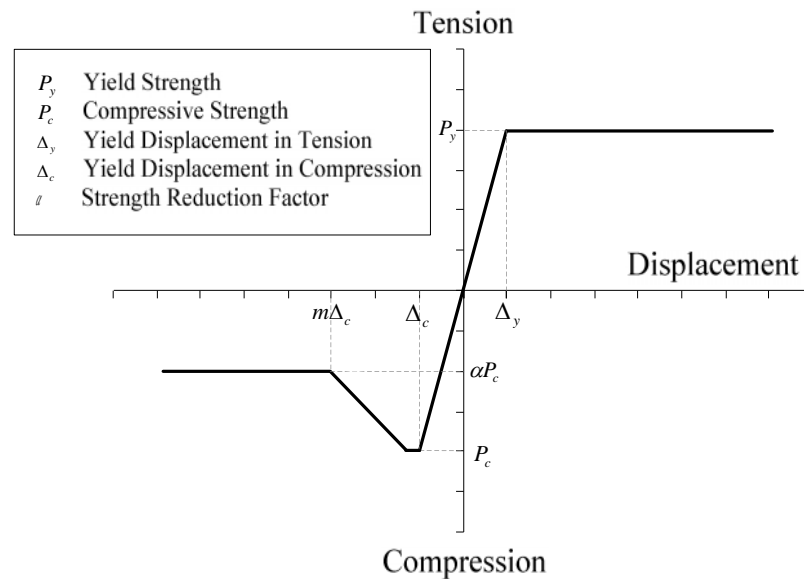


Figure 3.7 Backbone Curve of Regular-Buckling Braces.

3.2.6 Buckling-Restrained Braces (BRBs)

BRBs can be modeled by using a tri-linear force deformation relationship. The model can be implemented using Buckling Restrained Brace Bar in PERFORM-3D. This element consists of one inelastic and one elastic components that represent the yielding and transition zones of BRBs respectively. In this stage, yielding zone length was assumed to be 70% of the total length [12]. The members were assumed to have a deformation limit at 2.23% elongation when fracture occurs [23]. The backbone curve used in the modeling of BRB braces is shown in Figure 3.8.

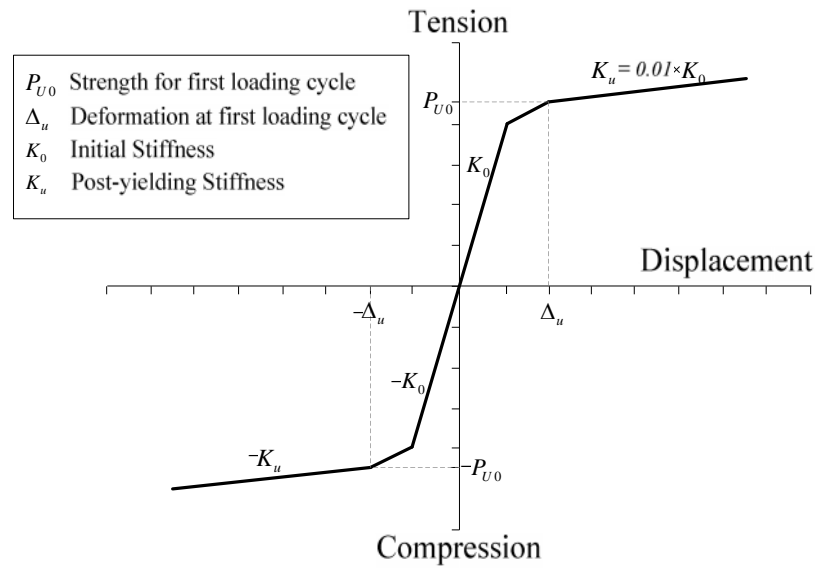


Figure 3.8 Backbone Curve of BRBs.

The BRB model was calibrated using test results carried out by Merritt et al. [12]. The steel hardening parameters for the BRBs were defined by calibrating the hysteretic models with the test result of specimen 2 in the above reference [12,23]. This model has been found to represent test results accurately as shown Figure 3.9.

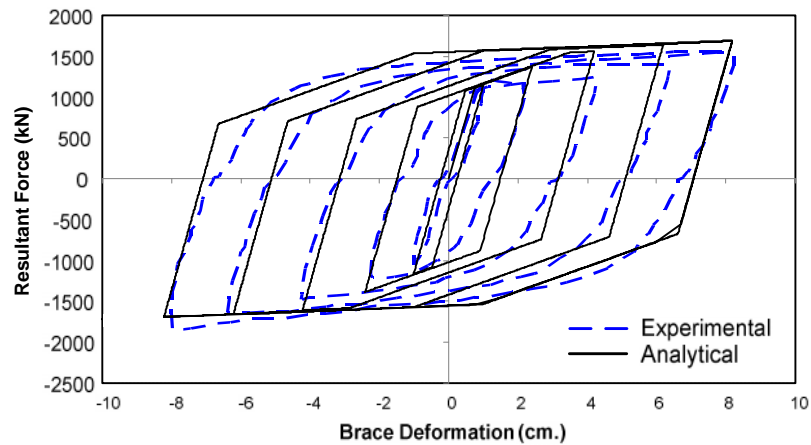


Figure 3.9 Hysteretic Model of BRBs.

3.3 Experimental Verification

3.3.1 PR connection Model

The component-based mechanical model of the PR connections with component behavior as discussed in sections 3.2.1 through 3.2.3 was verified by using the experimental result provided by Calado et al.[4]. The moment-rotation response of Specimen named BDD9 reported in Calado et al. [4] was selected for comparison with analytical results. The top, seat, and web angles are connect to the column (HEB160) and beam (IPE300) by bolts. Figure 3.9 shows the selected specimen. Angle sections L120×120×10 was used to connect the beam to the column. Top and seat angles were connected by 4 bolts (M16) arranged in two rows on column and beam flanges, while double web angles were connected by 3 bolts (M16), arranged in one column on the beam web and the column flange. Plates with 12 mm. thickness were used as stiffeners in the column panel zone.

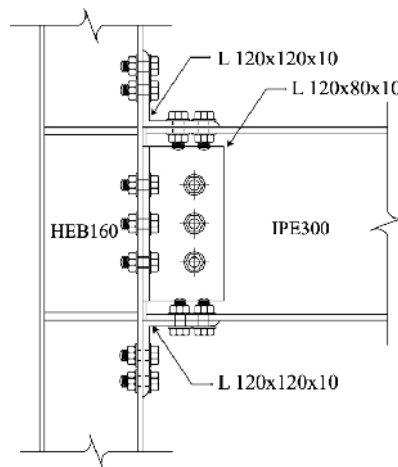


Figure 3.10 Test Specimen by Calado et al [4].

The experimental and analytical results are compared in Figure 3.11. The comparison shows that the mechanical model can predict the hysteretic response of the connection well in terms of stiffness and strength. The model demonstrates the pinching response which is the key characteristic of PR connections.

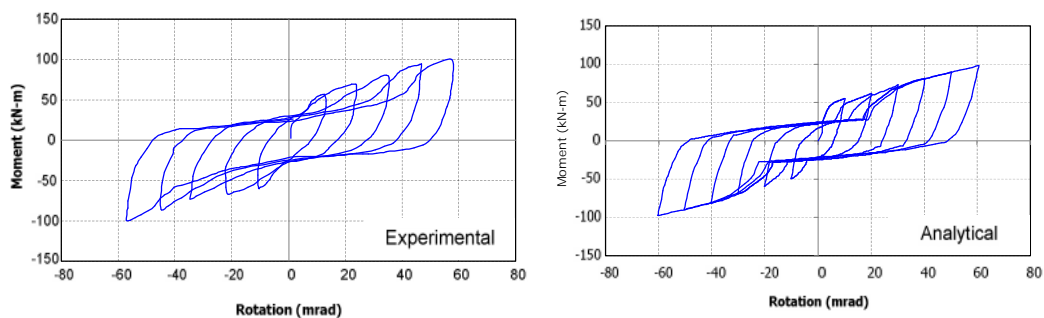


Figure 3.11 Experimental and Analytical Hysteretic Responses.

3.3.2 KBMF with PR connections Model

An analytical model using the repetitive assumptions mentioned in previous sections was created to represent the test frame described in section 2.4. The one-bay one-story test specimen was subjected to cyclic loading with gradually increasing displacement magnitude. The analytical model of the tested frame is illustrated in Figure 3.12 and Table 3.1 shows the section properties of the frame. Frame lines in the model represent the centerlines of the members.

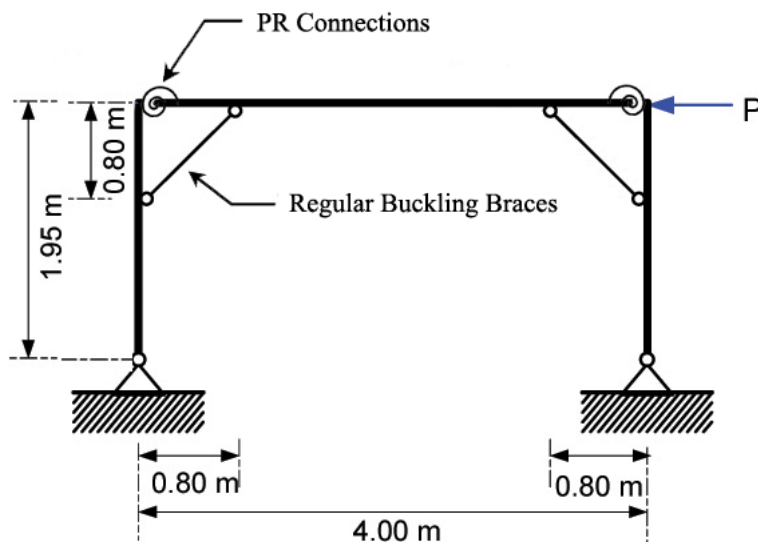


Figure 3.12 Analytical Model of Test Specimen.

Table 3.1 Section Properties of Frame.

Member	Section	Steel Grade
Beams	H250 × 125	A36
Columns	H250 × 250	A36
Knee Braces	Circular tube 76.2 × 3.9	A36

The beam-to-column joints consisted of top and seat angle connections. Three-parameter power model developed by Kishi and Chen [7] was employed to design the connections. Angle sections L150×150×13 and L100×100×13 were adopted for the top and seat angles, and web-angles, respectively. Both top and seat angles were connected by 4 M22 bolts, arranged in two rows on the column and beam flanges. For the web angles, 3 M16 bolts arranged in one column were used to connect the angle to the beam web. An analytical model of the specimen was created and analyzed using the same cyclic loading history from the test. Figure 3.13 shows the details of the PR connections in the KBMF test frame.

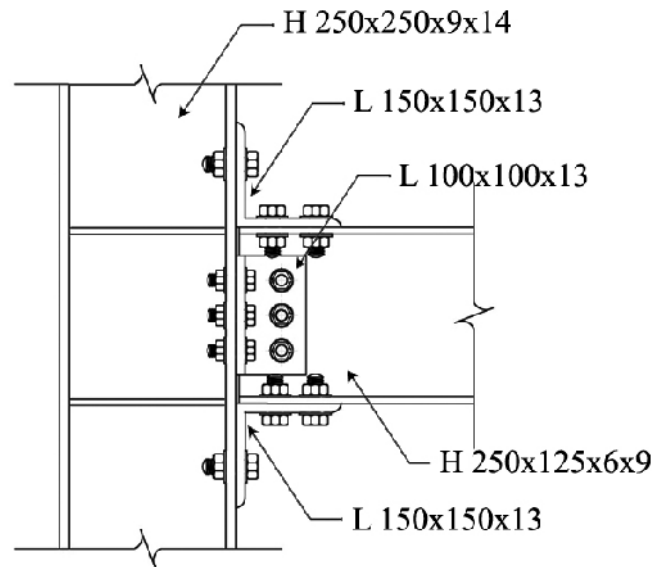


Figure 3.13 Top and Seat Angle Connections with Double Web Angles.

The results from the simulations were compared with the experimental results in Figure 3.14. As can be seen, the analytical model can well predict the overall hysteretic behavior of the KBMF with PR connections in terms of stiffness, strength, and pinching behavior. However, the stiffness of the model at 1-3% drift is larger than that from the experiment and the model provides only small pinching in the hysteretic loops. The analytical result shows that the pinching behavior is extremely difficult to model. In the analysis, the pinching behavior in the model is influenced only by nonlinear contact components at the joints.

In reality, the pinching may be a result from the combination of slippage at each bolt-hole in both the connections and the braces. Moreover, in the later stage of loading cycles, the local plastic deformation in the beam flange at the contact points between the beam and the ends of the braces was clearly evident. This local phenomenon was another source that caused pinching and reduction of the frame stiffness and was impractical to be included in the model. It was found that this localized plastic deformation and the bolt slippage affected the deformation of the knee braces and resulted braces having much smaller strain when compared to those from the analysis. Nevertheless, because the overall hysteretic loops are well captured by the model, the analysis should accurately provide the overall frame deformation values while some errors may be presented in localized response parameters.

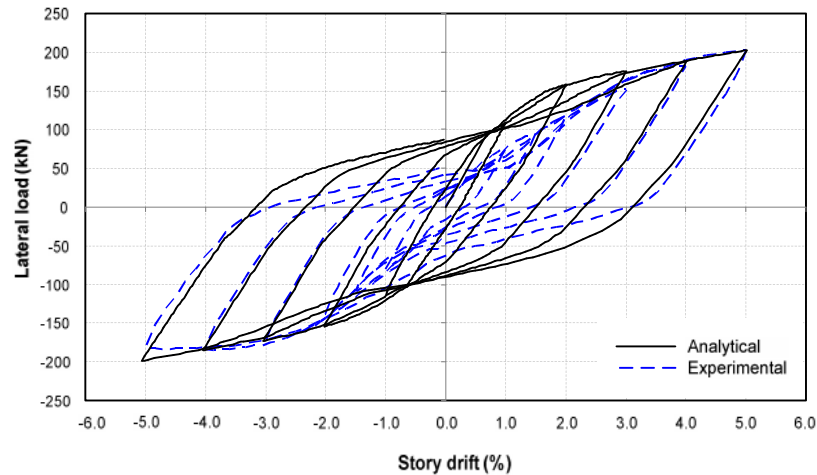


Figure 3.14 Simulation of Test Result.

3.4 KBMF with PR connections and BRBs

The test frame in the previous section was reanalyzed with the regular buckling braces replaced by BRBs. The yield strength of the braces was kept constant for both the buckling braces and BRBs. The hysteretic loops from the analysis of the frame with the two types of braces were compared in Figure 3.15.

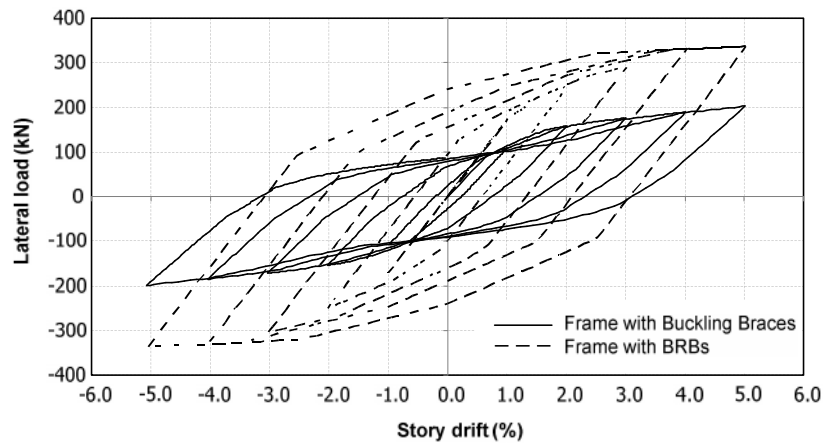


Figure 3.15 Comparison of KBMF Model with Different Type of Braces.

The results indicated that the frame with BRBs had both strength and stiffness larger than those of the frame with regular buckling braces. Based on the figure, the frame with BRBs has greater stiffness than that of the frame with conventional braces by approximately 60 percent, even though the cross sectional area of the braces is similar. In terms of strength, the lateral capacity of the frame with BRBs was significantly larger (approximately 65%) than that of the frame with regular braces. The regular buckling brace buckled in compression and experienced strength loss resulting in the overall strength loss of the frame. Figure 3.15 also indicates that the frame with BRBs had very stable hysteretic loops with excellent energy dissipation even with PR connections. The pinching behavior was not observed. The stable hysteretic response of the BRBs is the significant cause of the differences in the hysteretic shape of the two frames.

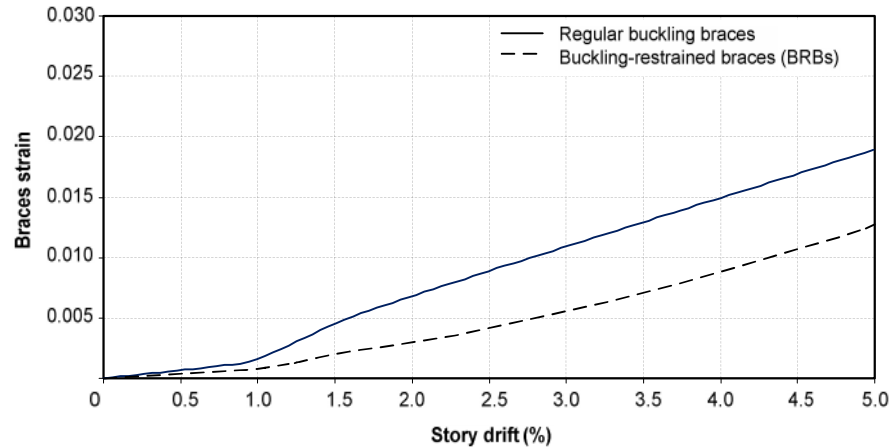


Figure 3.16 Strain in Knee Braces.

Figure 3.16 shows the strain values in the braces at different drift levels. As can be seen, the strain of the regular buckling brace is larger than that of the BRB. The flexibility of the connection in conjunction with the buckling of the regular brace resulted in significantly larger strain values when compared with the KBMF with rigid connections as can be deduced from the deformed shape shown in Figure 3.17. In the figure, the gray line and the black line represent the deformed shape of the KBMF with rigid connections and the KBMF with PR connections, respectively. For the left connection in the KBMF with PR connections, the joint opens up and results in additional tensile strain in the brace. On the other hand, the right connection closes resulting additional compressive strain in the brace. Because of the strain-hardening feature in the BRB, this additional rotation at the connection is significantly smaller for the frame with BRBs compared to that of the frame with conventional braces. It can be deduced that the regular brace in the frame with PR connections would eventually fracture under a smaller drift.

For the KBMF with BRB, the analytical results describing above indicate that the flexible of PR connections does not impact. The BRB can deform less than the regular braces when the roof drift is similar. This then leads to higher overall ductility of the frame with BRBs.

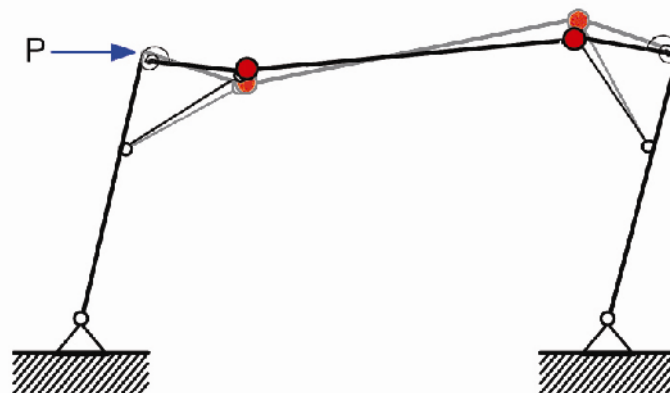


Figure 3.17 Mechanism of KBMF System.